ARL-TR-9779 ● SEP 2023

Quasi-static Tensile Response of Polymer Films and Metallic Foils

by C Allan Gunnarsson, Eric Wetzel, and Minghui Li

NOTICES

Disclaimers

The findings in this report are not to be construed as an official Department of the Army position unless so designated by other authorized documents.

Citation of manufacturer's or trade names does not constitute an official endorsement or approval of the use thereof.

Destroy this report when it is no longer needed. Do not return it to the originator.

ARL-TR-9779 ● SEP 2023

Quasi-static Tensile Response of Polymer Films and Metallic Foils

C Allan Gunnarsson and Eric Wetzel
DEVCOM Army Research Laboratory

Minghui Li
Army Educational Outreach Program (AEOP) Apprentice
Academy of Applied Science

REPORT DOCUMENTATION PAGE

1. REPORT DATE	2. REPORT TYPE	3. DATES COVERED	
		START DATE	END DATE
September 2023	Technical Report	4/01/2022	6/01/2023

4. TITLE AND SUBTITLE
Quasi-static Tensile Response of Polymer Films and Metallic Foils

5a. CONTRACT NUMBER	5b. GRANT NUMBER	5c. PROGRAM ELEMENT NUMBER
W9115R-15-2-0001		
5d. PROJECT NUMBER	**5e. TASK NUMBER**	**5f. WORK UNIT NUMBER**

6. AUTHOR(S)
C Allan Gunnarsson, Eric Wetzel, and Minghui Li

7. PERFORMING ORGANIZATION NAME(S) AND ADDRESS(ES)	8. PERFORMING ORGANIZATION REPORT NUMBER
DEVCOM Army Research Laboratory ATTN: FCDD-RLA-TB Aberdeen Proving Ground, MD 21005	ARL-TR-9779

9. SPONSORING/MONITORING AGENCY NAME(S) AND ADDRESS(ES)	10. SPONSOR/MONITOR'S ACRONYM(S)	11. SPONSOR/MONITOR'S REPORT NUMBER(S)

12. DISTRIBUTION/AVAILABILITY STATEMENT
DISTRIBUTION STATEMENT A. Approved for public release: distribution unlimited.

13. SUPPLEMENTARY NOTES
ORCID IDs: C Allan Gunnarsson, 0000-0002-8472-5193, Eric Wetzel 0000-0002-0176-3072

14. ABSTRACT
This report presents the quasi-static tensile properties of polyimide, polyethylene terephthalate, polyetherimide, 1100 series aluminum foil, and alloy 260 brass foil. Multiple methods for specimen fabrication were considered, including laser cutting, machining, water jetting, and blade cutting. For polymer films, the best results were achieved using a computer numerical–controlled blade cutter to produce dogbone–shaped specimens. For metal foils, no suitable means of dogbone fabrication were found, so manually blade-cut rectangular specimens were used. Digital image correlation was used for optical strain measurement in the gage section. The resulting tensile stiffness, strength, and elongation properties for films and foils are equal to or higher than previously published values, suggesting that the present methods are superior for characterizing intrinsic material response.

15. SUBJECT TERMS
polymer film, metal foil, tensile characterization, digital image correlation, film tensile specimen fabrication, polyimide film, PET film, Al foil, brass foil, PEI film, Terminal Effects

16. SECURITY CLASSIFICATION OF:			17. LIMITATION OF ABSTRACT	18. NUMBER OF PAGES
a. REPORT	b. ABSTRACT	C. THIS PAGE		
UNCLASSIFIED	UNCLASSIFIED	UNCLASSIFIED	UU	34

19a. NAME OF RESPONSIBLE PERSON	19b. PHONE NUMBER *(Include area code)*
C Allan Gunnarsson	(410) 306-1964

STANDARD FORM 298 (REV. 5/2020)
Prescribed by ANSI Std. Z39.18

Contents

List of Figures

List of Tables

1. Introduction

Many Army systems depend on films and foils with high stiffness and strength. As novel high-performance materials are developed, it is necessary to quantify their mechanical properties to understand their performance relative to conventional materials, and for use in design and simulation of material applications. High-stiffness and strength fibers are commonly used in textiles and composites, therefore considerable experimental method development for their tensile evaluation has been reported. Tensile testing methodology development for high-performance films and foils, however, has received less detailed attention. ASTM standards for polymer films (ASTM D882-18 2018) and metal foils (ASTM E345-16 2016) provide a foundation for testing. These ASTM methods are developed in part to support industrial qualification of materials and do not necessarily describe the most advanced characterization methods that can be applied to the evaluation of high-performance materials.

The objective of the present report is to evaluate methodologies for tensile testing of films and foils, recommend best practices, and collect high-quality tensile data for use in application modeling and experimental benchmarking for novel material development. Three polymer films and two metal foils are evaluated: polyimide film, polyethylene terephthalate (PET) film, polyetherimide (PEI) film, 1100 series aluminum (Al) foil, and alloy 260 brass foil. These materials were selected to provide a range of stiffness, strength, and toughness behaviors, with both elastic and plastic responses, allowing for identification of test methods with broad applicability.

Polyimide film has been characterized in tension (Roe and Baer 1972; Askins 1985; Miyauchi et al. 2011; Zhang et al. 2012; Shen et al. 2016; Liu and Liu 2022). The tensile properties of PET (Stearne and Ward 1969; Bhushan et al. 2002) and Al foil (Klein et al. 2001; Connolley et al. 2005; Zhou et al. 2007) have also been reported. Several studies have demonstrated that for films, specimen thickness can play a significant role in the material properties that are observed (Kumar et al. 2016; Zheng et al. 2020).

This report introduces two improvements to film tensile testing that are not commonly implemented. First, a wide range of film and foil cutting methods are evaluated to determine suitability for creating dogbone shapes and their ability to create smooth edges with low defect population. Specimen edge smoothness is key for achieving maximum strength and elongation. Second, digital image correlation (DIC) (Schreier et al. 2009) is used to visually map strain fields in the gage section

of test specimens, rather than relying on machine displacement, extensometers, or strain gages, which provide much more limited data.

2. Methods

2.1 Materials

Five materials were used here for tensile experiments, all sourced commercially from an industrial supply company, and all obtained in nominal 0.0508-mm (0.002-inch) thickness. The first three materials were polymer films: polyimide, produced by DuPont and available commercially under the trade name Kapton HN; PET, produced by Grafix Arts and available commercially under the trade name Dura-Lar Clear; and PEI, available commercially under the trade name Ultem. In addition to the three polymers, two metallic foils were used: Al foil alloy 1100 and brass alloy 260. The Al foil was temper H19 and the brass foil half hard. The PET, PEI, brass foil, and Al foil came in roll form allowing machine (or roll) direction (MD) specimens to be fabricated parallel to the roll and transverse direction (TD) specimens perpendicular to the roll. For the polyimide film, the material came as square film pieces, so the MD and TD were not obvious; however, close inspection of the film showed features aligned in one direction. It was presumed that this alignment corresponded to the original MD from the roll that the square pieces were cut from, and so the specimens fabricated in the MD for this material were aligned with those features.

2.2 Specimen Fabrication

ASTM standard D882-18 (2018) covers tensile experiments for polymer films. This standard references a separate standard covering the fabrication of test specimens, ASTM D6287-17 (2017), which directs researchers to use a dual-shear cutter for fabrication of rectangular specimens of 5.0- to 25.4-mm width and minimum 50-mm gage length. ASTM standard E345-16 (2016) covers tension testing of metallic foil and directs experimenters to also fabricate specimens using a double-shear cutter or mill dogbone–shaped specimens out of a stack of foil layers. It was not possible to access a dual shear cutter for specimen fabrication. However, several specimen fabrication techniques were investigated for suitability, including rectangular specimens fabricated using a razor blade, replicating the outcome of the method in the ASTM standard. Other methods of specimen fabrication were evaluated and are discussed later.

Two types of specimen geometry were used for tensile experiments: rectangular and dogbone. Rectangular specimens have a constant width in the grip and gage

length areas, while dogbone specimens have a larger width in the grip area that tapers down to a narrower width in the gage length. Dogbone–shaped tensile specimens are ideal, with stress concentration in the specimen away from the grip-specimen interface. However, the ASTM standards recommend rectangular specimens for their ease of preparation and interpretation of elongation using only a far-field displacement measurement. Typical specimen shapes that were used for this study are shown in Fig. 1.

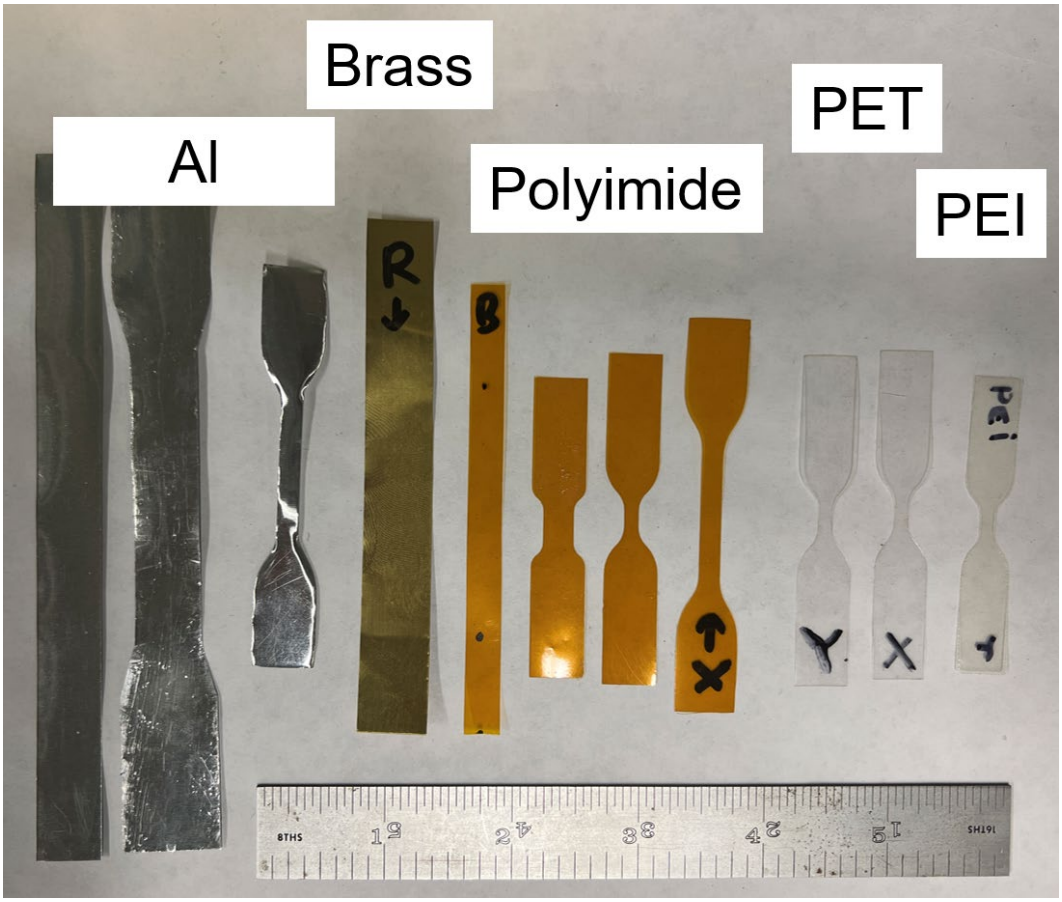

Fig. 1 Typical rectangular and dogbone specimens left to right: Al foil (silver), brass (gold), polyimide (amber), PET (clear, second and third from right), PEI (clear, right-most only). Scale marked in inches.

For the brass and Al foils, the rectangular paper cut specimens were 75 mm (3 inch) long, with a gage length of 37.5 mm (1.5 inch) and gage width of 12.7 mm (0.5 inch). For the razor blade cut polymer films, the total length and gage length were the same as the rectangular foil specimens; the gage width was 6.35 mm (0.25 inch). The bladed computer numerical control (CNC) cut dogbone polymer film specimens had a grip width of 9.375 mm (0.375 inch); this transitioned via two radii down to a gage width of 3.2 mm (0.125 inch) and gage length of 3.2 mm (0.125 inch).

2.3 Tensile Experiments

Tensile experiments were performed on the film and foil specimens using a servo-hydraulic test machine (Instron 8871) with wedge grips (Fig. 2). Tensile experiments on the rectangular geometry specimens used 600-grit emery paper as a liner between grip and specimen, as recommended by the testing standard to mitigate specimen slip and promote specimen failure away from the grip-specimen interface. Four to five specimens were completed for each material and fabrication technique to ensure repeatability and context for any outliers. LED lighting was used for specimen illumination to prevent any external specimen heating.

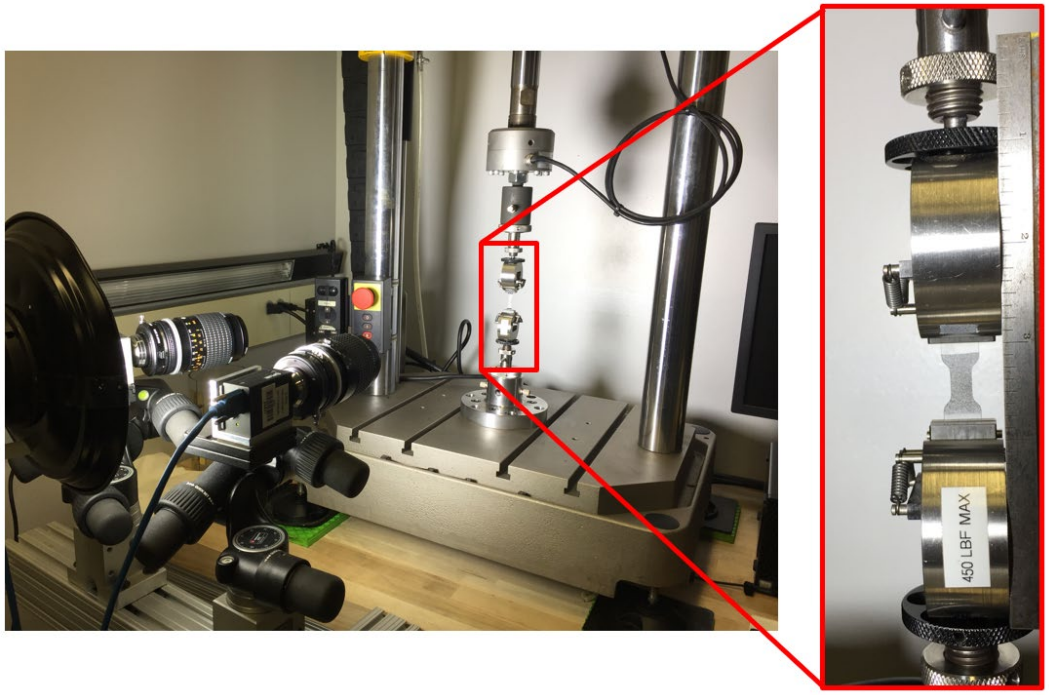

Fig. 2 Film tensile specimen (dogbone) loaded into test machine grips (scale at right marked in inches)

Two-dimensional DIC was performed on all tensile specimens, using white paint base and black paint speckles. Paint was applied only to the specimen gage section. Optical framing cameras (FLIR Grasshopper GS3-U3-23S6M-C) were used to image the specimens during loading. DIC postprocessing was performed using commercially available software (Correlated Solutions VIC2D).

For the experiments documented here, the engineering strain tensor was used for DIC analysis. This data was used to compare material properties from other reference and literature sources. Many of these sources do not explicitly define the strain type provided, listing only elongation; it is assumed that the simplest definition is used, as many of these sources are likely using the very basic global

deformation measures defined in the testing standard and not utilizing optical or full-field strain measures. It should be noted that for tension experiments with large elongations, conversion to true stress representing actual specimen cross-sectional area at failure would be more accurate and would increase the strengths reported. However, to maintain consistency with the techniques employed by other studies, engineering stress is reported. The term yield is used here to differentiate between elastic and plastic behavior. Determination of the yield point, for quantification of yield stress and strain, uses a 0.2% strain offset.

The use of DIC in strain measurement allows for increased accuracy by removing any portion of the global deformation measurement that is responsible for specimen slip, and, for the dogbone–shaped specimens, accounts for any specimen deformation that occurs outside of the gage length. For these experiments, unless otherwise stated, the strain was obtained using an average over the entire specimen gage length. The strain rate for these experiments was nominally 0.001/s, using the gage length to prescribe a constant test machine velocity. The strain rate was then quantified for each experiment by taking a linear fit of the strain–time data. For all materials except PEI, this strain rate was relatively constant, and resulted in an engineering strain rate of 0.0007–0.002/s. However, for the PEI experiments, the strain rate increased significantly after yield, reaching 0.01/s.

3. Evaluation of Specimen Fabrication Techniques

Several different techniques were evaluated for specimen fabrication: laser cutting, waterjet cutting, punch cutting, razor blade cutting of a dogbone geometry using a hardened steel template, blade cutting of dogbone geometry using a CNC machine, and milling of dogbone geometry from stack of layers. Table 1 shows the techniques that were used for each material; not all techniques were used, as they may have been eliminated due to earlier results. For example, after waterjet cutting of polyimide film revealed specimens with bad edge quality, it was not repeated for the other polymer films.

The following sections document the effect of different specimen fabrication techniques for each material. In general, higher elongation was correlated with smoother specimen edges in the gage length. These smoother edges contained fewer and smaller defects and notches, therefore increasing the fracture toughness of the specimen. This reduced edge defect population is critical for quantification of the maximum values representing the intrinsic material elongation and strength. For materials such as polyimide and PET that did not exhibit strain concentration and neck formation after yield, increasing elongation was directly correlated with increasing strength.

Table 1 Summary of fabrication techniques for all five materials

Technique	Polyimide	PET	PEI	Al foil	Brass foil
Laser cutting (dogbone)	**X**	**X**	**X**	**X**	…
Waterjet cutting (dogbone)	**X**	…	…	**X**	…
Punch cutting (dogbone)	**X**	…	…	**X**	…
Razor blade with template (dogbone)	**X**	…	…	…	…
Bladed CNC machine (dogbone)	*	*	*	**X**	…
Razor blade (rect)	**X**	…	…	**X**	…
Razor blade (rect) with emery paper grip liner	**X**	**X**	**X**	…	…
Paper cutter (rect)	…	…	…	*	*
Milled from foil layer stack (dogbone)	…	…	…	…	…

Notes: X = did not work well
… = did not evaluate
* = worked well, used for final results

One method that was not attempted for the metal foils but should be considered for future study is wire electrical discharge machining (EDM). EDM can produce smooth edges with high resolution in electrically conductive materials, including metal foils, and could produce dogbone–shaped specimens (Mouralova et al. 2022). A challenge for EDM machining will be supporting the foils during cutting and providing a threading path for the wire that does not require tedious manual threading for each sample.

3.1 Polyimide Film

Polyimide film is the benchmark material of highest interest, as this material is expected to be similar in behavior to novel high-performance polymer films currently in development. Therefore, an exhaustive attempt was made to find the fabrication technique that resulted in consistent results that best approached intrinsic material mechanical response. The following techniques were used to fabricate tensile specimens:

- Laser cutting dogbone specimens
- Razor cutting rectangular specimens (both with and without emery paper liners in grip)
- Razor cutting dogbone specimens using a hardened steel template
- Bladed CNC machine cutting dogbone specimens
- Waterjet cutting dogbone specimens
- Punch cutting dogbone specimens

Laser cutting was performed using an Epilog 30-W CO_2 laser cutter. During laser cutting, the polyimide film burned and charred, which created a very rough and

jagged specimen edge. The Cricut Maker three-bladed CNC cutting machine was used to cut the polyimide film, as well as the other polymer films, into dogbone specimens. Waterjet cutting of the polyimide film into dogbone specimens was accomplished using a stack of three polyimide film layers clamped between sacrificial rigid polycarbonate (PC) plates (9.4 mm thick).

Figure 3 shows stress–strain data from representative experiments for each fabrication technique attempted for polyimide film, as well as microscopy images of the specimen edge for that technique. For the different fabrication techniques, the elastic and yield behavior are similar, and the mechanical responses overlap as they extend to failure. However, the elongation and tensile strength for the different techniques have large variability, with the techniques that produced the smoothest edges having the highest elongation; this correlation is observed by comparing the microscopy image of fabrication technique to the elongation. The failure behavior of this material appears to be controlled by flaw defect presence and size in gage length edge.

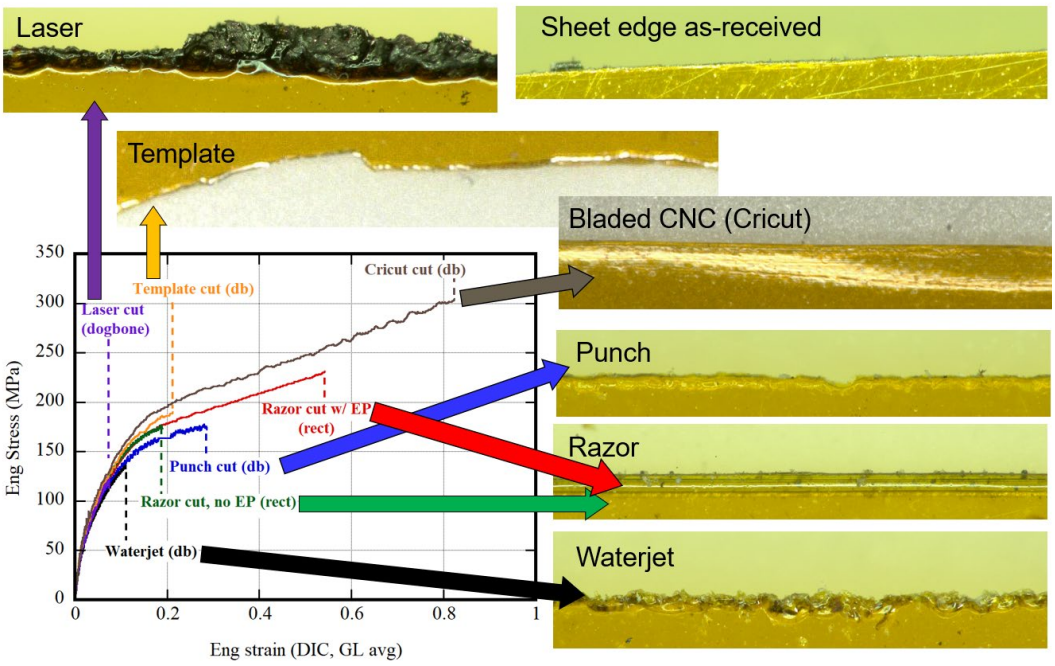

Fig. 3 Edge smoothness effect on material response and elongation for polyimide film. Dogbone specimens are labeled as "dogbone" or "db," while rectangular specimens are labeled "rect."

The ASTM governing tensile experiments of plastic film mention that the use of emery paper as a liner in the grips can reduce premature specimen failure; the present results indicate that the use of emery paper did improve test results, increasing elongation from 18% to 45%. For the polyimide film, the bladed CNC cut dogbone specimens had smooth edges and dogbone shape, which resulted in

the highest elongation of all fabrication techniques. That elongation met or exceeded the reference elongation provided by the manufacturer.

3.2 PET Film

The following fabrication techniques were attempted on specimens for PET film:

- Laser cutting dogbone specimens
- Razor cutting rectangular specimens
- Bladed CNC machine cutting dogbone specimens
- Punch cutting dogbone specimens

The PET film melted when laser cut, resulting in very smooth edges. This was a different result compared to the laser-cut polyimide film, which burned and charred. However, laser cutting the PET created a heat affected zone at the specimen edge that likely reduced the elastic modulus when compared to other fabrication techniques. In addition, the melting and cooling process from cutting may have created a thicker specimen at the specimen edge, artificially inflating the elongation. The bladed CNC-cut dogbone specimens had similar modulus to the razor-cut specimens and higher elongation. Figure 4 shows microscopy images of PET film for the different fabrication techniques.

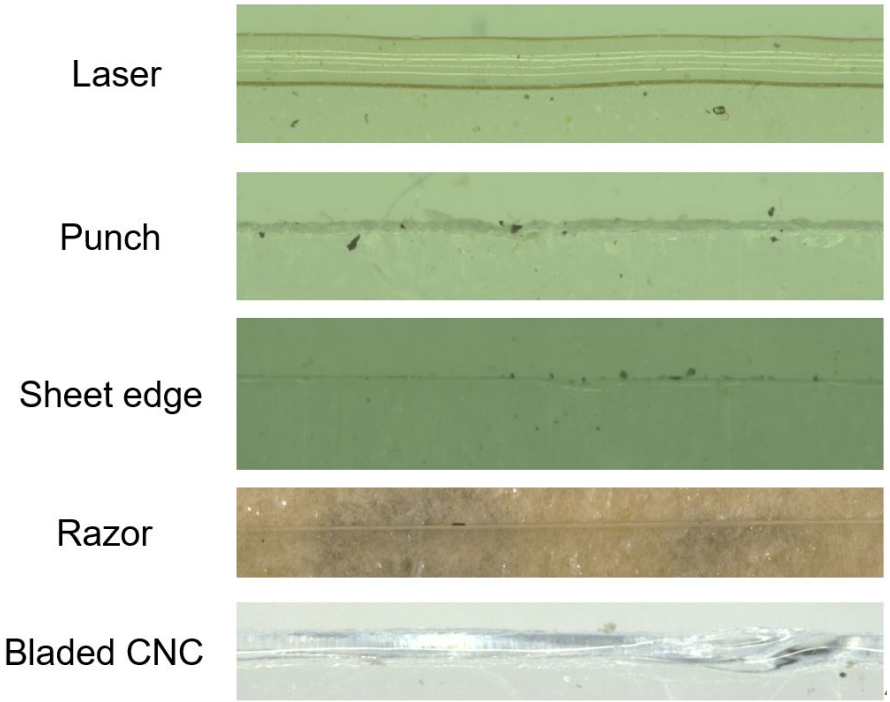

Fig. 4 Specimen edge microscopy for PET specimens

3.3 PEI Film

The following fabrication techniques were attempted on specimens for PEI film:

- Laser cutting dogbone specimens
- Razor cutting rectangular specimens
- Bladed CNC machine cutting dogbone specimens

When laser cut, the PEI film burned and charred, similar to the polyimide film; only the razor and bladed CNC machine–cut specimens were tested. The elastic and yield properties for both techniques were very similar, while the elongation for the bladed CNC machine–cut specimens was much higher than the razor-cut specimens, matching the elongation listed for PEI in the literature. Figure 5 shows microscopy images of PEI film for the different fabrication techniques.

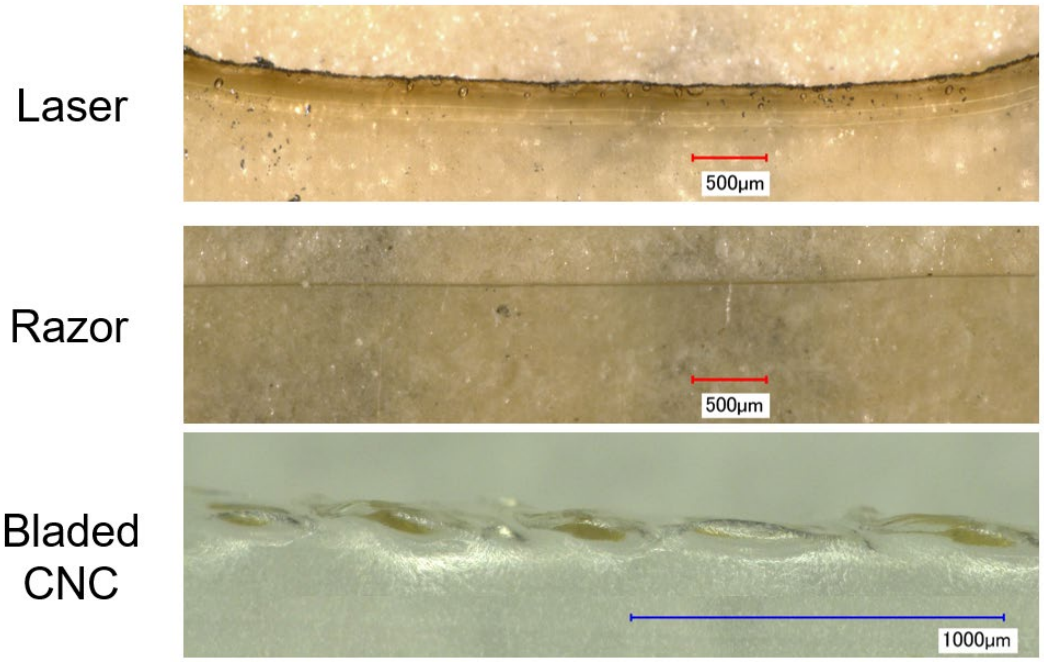

Fig. 5 Specimen edge microscopy for PEI specimens

3.4 Al Foil

The Al foil was not able to be cut using the bladed CNC machine or laser cutter. The following fabrication techniques were attempted on specimens for Al foil:

- Punch cutting dogbone specimens
- Paper cutter cutting rectangular specimens
- Mill cutting dogbone specimens from a foil layer stack

- Waterjet cutting dogbone specimens
- Razor cutting rectangular specimens

A stack of three Al foil layers was clamped between sacrificial rigid PC plates (9.4 mm thick), and from this assembly, dogbone specimens were milled using a CNC commercial-grade mill as suggested in the metallic foil tensile testing standard ASTM E345-16 (2016). However, the specimen edge quality for these specimens was very low, with numerous jagged edges and tears. Similarly, the waterjet-cut specimens had very rough specimen edges. The razor-cut specimen edges were mostly smooth, but not as smooth as the paper-cut specimens, so they were not tested. Figure 6 shows microscopy images of the Al foil specimen edges for each of the fabrication techniques. Tensile experiments were conducted on the punch-cut (dogbone) and paper-cut (rectangular) Al foil specimens. Punch cutting of the Al foil appeared promising, with relatively smooth edges (smoother than mill or waterjet, and just rougher than paper cut); however, during tensile testing, the elastic modulus obtained for the punch-cut specimens was lower than the paper-cut specimens and reference values for this material (34.7, 65.6, and 69.1 GPa, respectively).

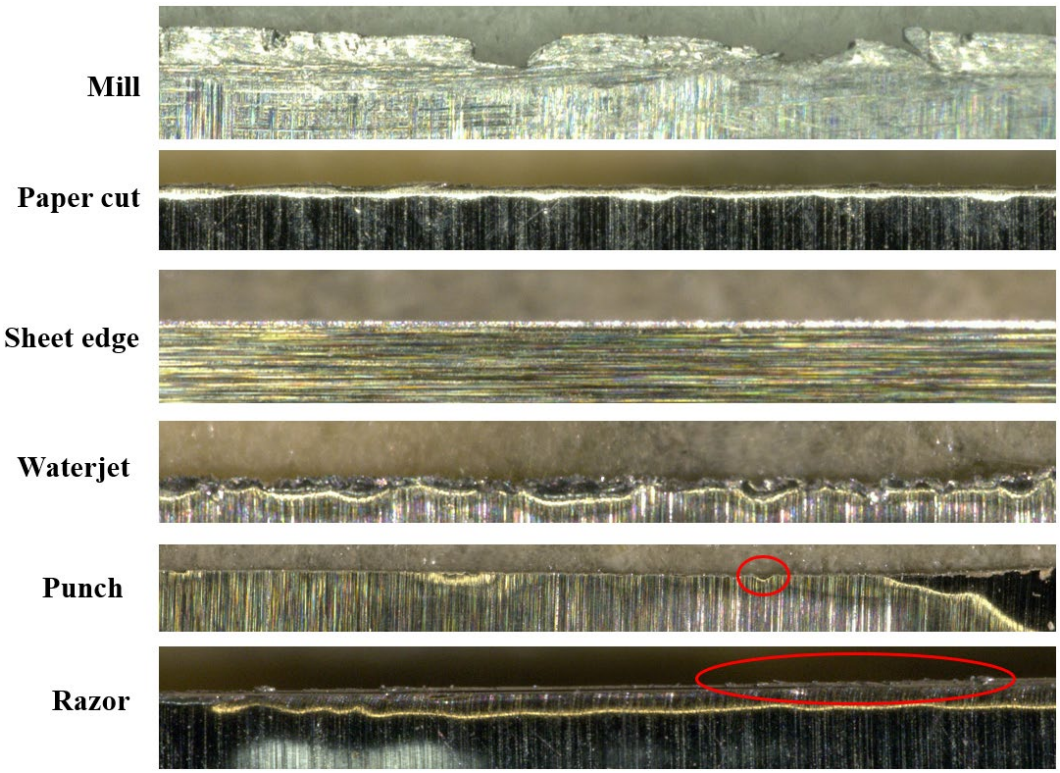

Fig. 6 Specimen edge microscopy for Al foil specimens

As can be seen in the microscopy image for the punch-cut Al foil, small defects were introduced into the specimen edge during fabrication. These small defects caused strain nonuniformity during the global elastic response of the tensile specimen. Figure 7a shows the material response for two MD Al foil specimens: one fabricated using the punch cutter and one fabricated using the paper cutter. Figures 7b and 7c show the strain distribution during elastic loading at a global stress of 56 MPa, within the elastic region of the material response, for the paper-cut specimen and the punch-cut specimen, respectively. The paper-cut specimen has a very uniform strain distribution, with a maximum of 0.5% strain. The punch-cut specimen has a nonuniform strain distribution, with regions at the edge reaching 4%.

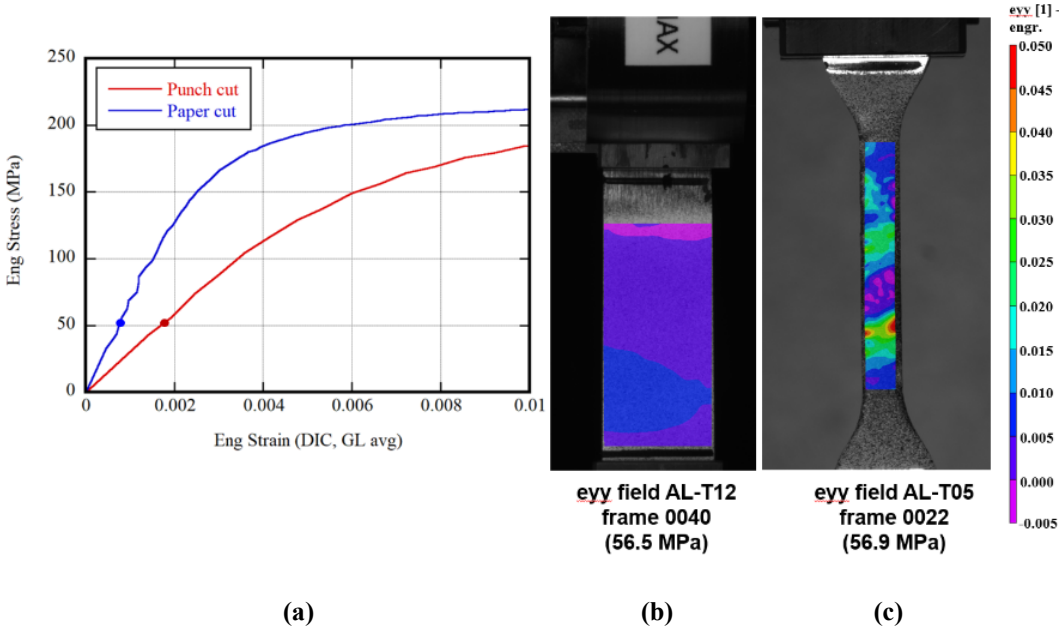

Fig. 7 (a) Material response for paper- and punch-cut Al foil specimens. Tensile strain profiles for (b) paper-cut and (c) punch-cut specimens at eng stress of 56 MPa for the two specimen data in (a). The strain color maps are the same for both (b) and (c). The two dots on each data in (a) indicate stress level of strain map shown in (b) and (c).

3.5 Brass Foil

The brass foil was not able to be cut using the bladed CNC machine, laser cutter, or razor blade. The only fabrication technique used for the brass foil specimens was paper cutting of rectangular specimens. Figure 8 shows the brass foil specimen edges as paper cut and as received on the material roll.

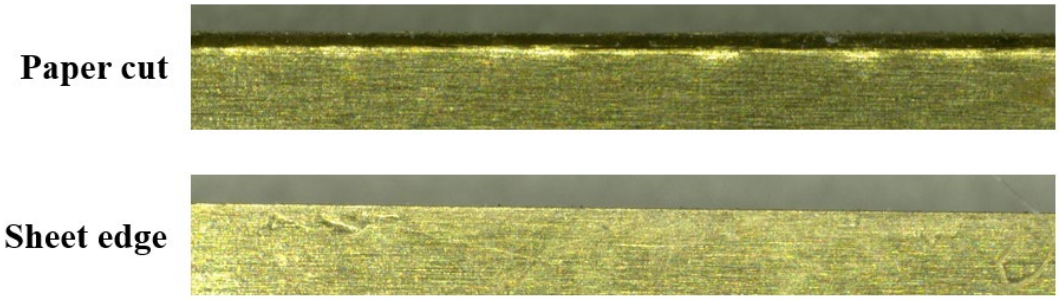

Fig. 8 Specimen edge microscopy for brass foil specimens

4. Results

Table 2 summarizes the material properties obtained for each of the five materials documented here. The Kapton, PET, and PEI data were generated using dogbone samples cut with the CNC bladed cutter. The Al and brass data were collected using rectangular paper-cut specimens. Three of the materials—polyimide film, PEI film, and Al foil—were isotropic, with little difference in material properties between MD and TD orientations. The PET film and brass foil were anisotropic with tensile properties affected by specimen orientation. Therefore, Table 2 contains separate properties for MD and TD orientations for both the PET film and brass foil.

Table 2 Summary of tensile material properties for all five materials

Material		Modulus (GPa)	Yield strength (MPa)	Yield elongation (%)	Strength (MPa)	Elongation (%)
Kapton		3.9	59.9	1.72	297.3	86.8
PET	MD	4.5	90.2	2.17	190.7	147.3
	TD	5.6	92.3	1.85	240.3	91.0
PEI		3.1	68.7	2.42	103.9	58.6
Al foil alloy 1100		65.5	199.2	0.51	218.5	3.2
Brass alloy 260	MD	105.9	316.2	0.51	388.3	8.0
	TD	88.8	274.5	0.51	334.2	4.4

4.1 Polyimide Film

The polyimide film exhibited isotropic behavior in tension. For the bladed CNC machine-cut and razor blade–cut with emery paper specimens, there were no significant differences in the elastic and yield properties. Figure 9 shows the material response results for the four polyimide tensile experiments using bladed CNC machine cut specimens in the (a) MD and (b) TD orientations.

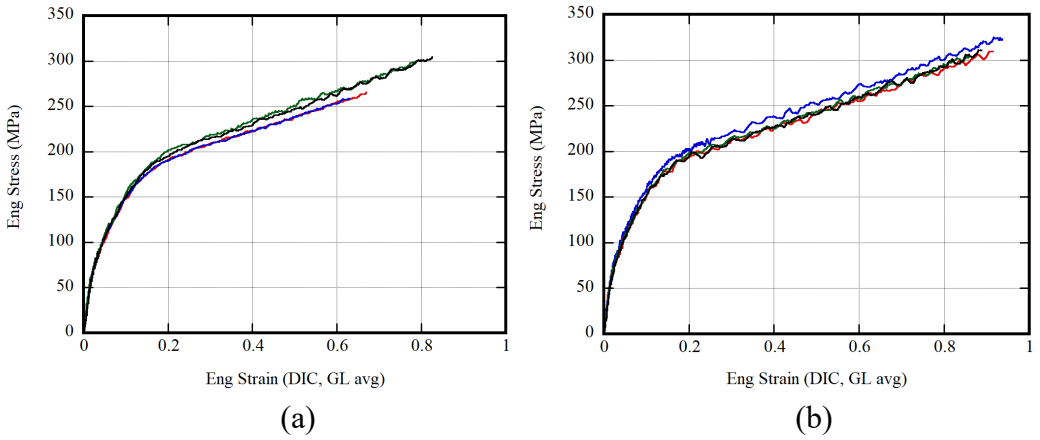

Fig. 9 Material response for tensile specimens of bladed CNC machine-cut polyimide in (a) MD and (b) TD orientations

During loading, the polyimide film exhibited good strain uniformity up to failure. There was no evidence of strain concentration or necking. Figure 10 shows the gage length strain distribution at the image just prior to failure for a typical polyimide specimen in the MD orientation. The gage length–averaged elongation for this experiment was 93%, and the strain range for the entire gage length was approximately ±5% (90%–99%). In Fig. 10, and subsequent DIC strain profile figures, the strain label is unitless, and is multiplied by 100 to represent the strain percentage discussed (e.g., the strain map range in Fig. 10 is 90%–100%).

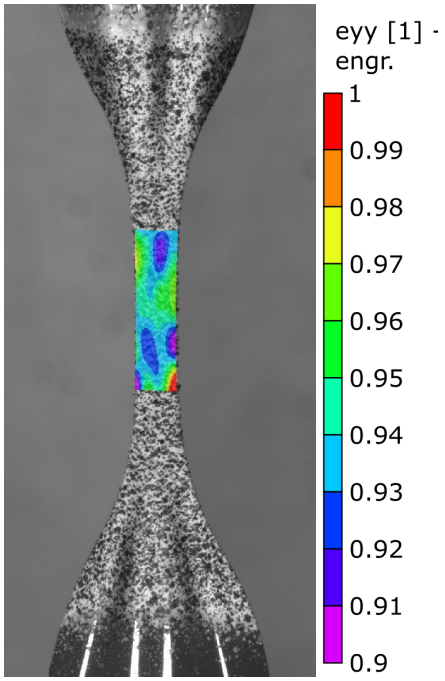

Fig. 10 Strain profile for typical polyimide-bladed CNC machine–cut tensile specimen just before failure. This specimen orientation was MD.

Table 3 summarizes the tensile properties of polyimide film from this study, as well as reference and literature values from other studies and sources. The referenced studies and sources did not claim use of optical methods to quantify specimen strain or perform a detailed examination of specimen fabrication technique and its effect on specimen edge quality.

Table 3 Summary of tensile material properties for polyimide film from this study and literature

Source	Orientation (if given)	Modulus (GPa)	Yield stress (MPa)	Yield elongation (%)	Strength (MPa)	Elongation (%)
This study	MD	3.85	62.3	1.77	313	90.0
	TD	3.95	57.9	1.68	282	72.7
Liu and Liu (2022)	MD	2.30	27.0	1.30	160	52.0
	TD	2.30	19.0	0.85	135	70.0
Miyauchi et al. (2011)	…	3.30	…	…	158	38.5
Askins (1985)	…	…	…	…	225–238	52.9–54.2
Shen et al. (2016)	…	…	…	…	254	59.9
Zhang et al. (2012)	…	3.19	46.6	…	264	67.1
Manufacturer datasheet (Kapton HN, 2 mil) (DuPont Kapton n.d.)	…	2.76	…	…	231	82.0
MatWeb Kapton polyimide film, 50 µm (n.d.)	MD	2.80	69.0	…	221	75.0

4.2 PET Film

The PET film exhibited significant anisotropy in tension. For all three fabrication techniques, the modulus, strength, and yield strength were lower and the elongation was higher in the roll direction. This behavior results from the manufacturing process, where the film is first drawn in one direction and then drawn in the second (transverse) direction (Bhushan et al. 2002). Additionally, the material response in the MD orientation (Fig. 11a) for PET exhibited strain-hardening post-yield (where stiffness increased approaching failure), while softening was observed post-yield in the transverse orientation (Fig. 11b).

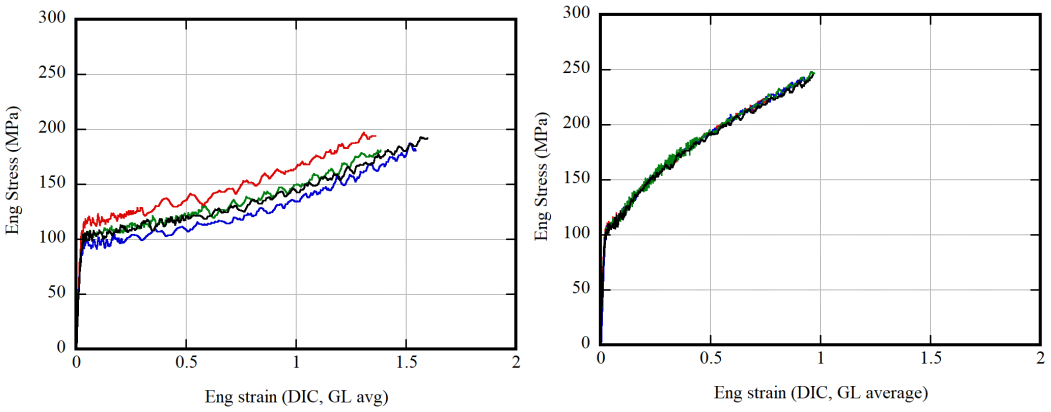

(a) (b)

Fig. 11 Material response for tensile specimens of bladed CNC machine-cut PET in (a) MD and (b) TD orientations

During loading, the PET exhibited good strain uniformity up to failure. Figure 12 shows the gage length strain distribution at the image just prior to failure. The gage length averaged elongation for this MD experiment was 154%, and the strain range for the entire gage length was approximately ±10% (142%–163%).

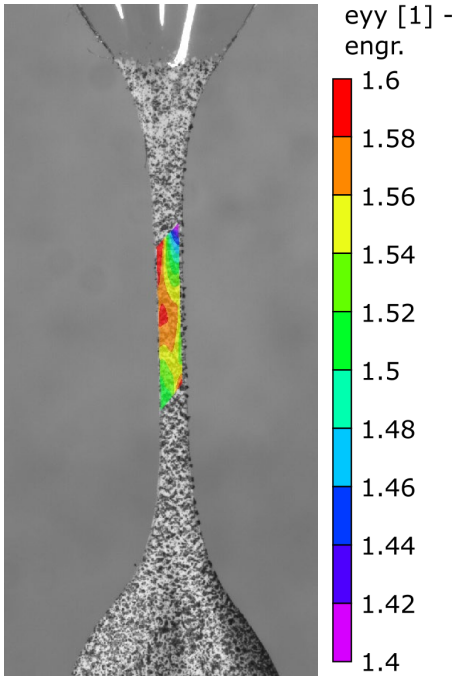

Fig. 12 Strain profile for typical PET-bladed CNC machine–cut tensile specimen just before failure. This specimen orientation was MD.

Table 4 summarizes the tensile properties of PET film from this study, as well as reference and literature values from other studies and sources. The referenced studies and sources did not claim use of optical methods to quantify specimen strain

or perform a detailed examination of specimen fabrication technique and its effect on specimen edge quality.

Table 4 Summary of tensile material properties for PET film from this study and literature

Source	Orientation (if given)	Modulus (GPa)	Yield stress (MPa)	Yield elongation (%)	Strength (MPa)	Elongation (%)
This study	MD	4.5	90.2	2.2	190.7	147
	TD	5.6	92.3	1.9	240.3	91
DuPont Mylar datasheet (2003), 92-gauge (0.92 mil thickness)	MD	4.9	…	…	199.9	116
	TD	5.1	…	…	234.4	91
Bhushan et al. (2002) standard PET 0.55 mil thickness (0.1/min)	…	3.3	…	…	158.0	39
ASTM D882-18 (2018), PET (0.9 mil thickness)	…	4.6	…	…	…	…
ASTM D882-18 (2018), PET (2.5 mil thickness)	…	…	99.2	5.2	211.0	…
MatWeb, Mylar film (n.d.), 200-gauge (2 mil thickness)	MD	3.5	…	…	193.0	135
	TD		…	…	228.0	110

4.3 PEI Film

During loading, the rectangular PEI specimens exhibited a neck and spread behavior where, post-yield, the material would first form a small, localized region of necking. Then, the neck would start to spread along the gage length until failure. The bladed CNC machine–cut dogbone specimens had a much shorter gage length than the rectangular specimens; during loading, the neck began to form almost immediately post-yield as well; however, there was no evidence of the neck spreading. The elongation was much higher for the dogbone specimens, matching reference values. The elongation values for the rectangular specimens were lower, even looking at the strain only at the neck or failure notch location. The dogbone specimen failure also exhibited stable crack growth, where a notch would begin to form and slowly grow across the specimen gage length. Figure 13 shows the material response results for the four PEI tensile experiments using bladed CNC machine–cut specimens in the (a) MD and (b) TD orientations. Figure 14 shows the

gage length strain distribution at an image just prior to failure notch formation. The gage length averaged elongation for this TD experiment was 66%, and the strain range for the entire gage length was approximately ±3% (69%–63%).

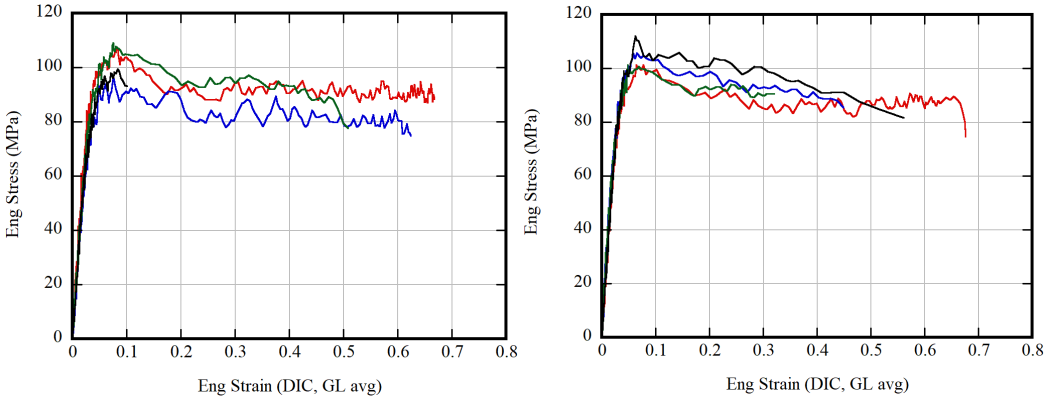

Fig. 13 Material response for tensile specimens of bladed CNC machine–cut PEI in (a) MD and (b) TD orientations

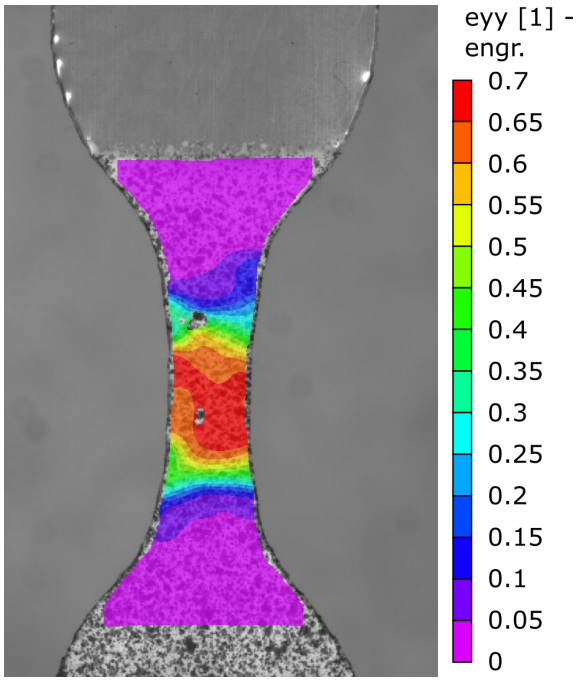

Fig. 14 Strain profile for typical PEI-bladed CNC machine–cut TD tensile specimen just before failure

Table 5 summarizes the tensile properties of PEI film from this study, as well as reference and literature values from other studies and sources. The referenced studies and sources did not claim use of optical methods to quantify specimen strain

or perform a detailed examination of specimen fabrication technique and its effect on specimen edge quality. The results obtained here almost exactly match the PEI reference study (Johnson and Burlhis 1983), except for yield stress. It is likely that this difference is due to methodology; here, a 0.2% offset was used to determine the yield point, while they likely used the maximum stress.

Table 5 Summary of tensile material properties for PEI film from this study and literature

Source	Orientation (if given)	Modulus (GPa)	Yield stress (MPa)	Yield elongation (%)	Strength (MPa)	Elongation (%)
This study	MD TD	3.2 3.0	69.7 67.8	2.4 2.5	104.9 102.9	59.1 58.0
Chirkov et al. (2016) drying, all strain %	…	2.14–2.81	77–89	…	78–111	…
Johnson and Burlhis (1983)	…	3.0	105.0	…	105.0	60.0
MatWeb Quantum PEI – Ultem (n.d.)	…	3.0	…	…	105.0	60.0
Ultem PEI film datasheet (CS Hyde Company n.d.)	…	3.3	…	…	98.0	52.0

4.4 Al Foil

The Al foil exhibited isotropic behavior in tension with no significant difference between the elastic and yield properties. Figure 15 shows the material response results for the four Al foil tensile experiments using paper-cut specimens in the (a) MD and (b) TD orientations. The tensile properties obtained here are approximately the same as the reference properties given for this material.

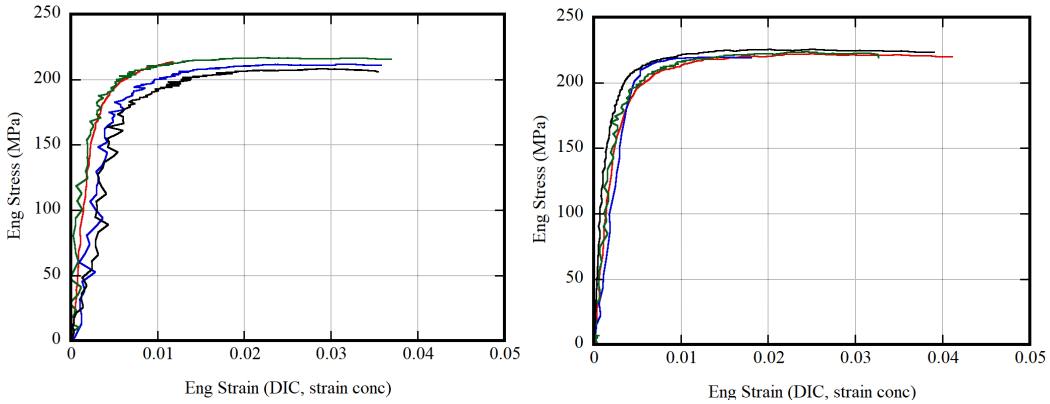

Fig. 15 Material response for tensile specimens of paper-cut Al foil in (a) MD and (b) TD orientations

The Al foil specimens exhibited strain concentration in the gage length as failure approached and had less evenly distributed strain fields just before failure. Strain for these experiments was extracted in two ways: an average over the entire gage length and an average over a small area at the strain concentration location. The elastic and yield properties measured using both strain measures were the same and similar to reference values for this material. Elongation obtained at the strain concentration matched the reference values and is therefore used. Figure 16 shows the gage length strain distribution at the time just prior to failure for one MD Al foil experiment. In the figure, the larger white box represents the gage length areal average, while the smaller white box represents the area where the strain concentration data is obtained.

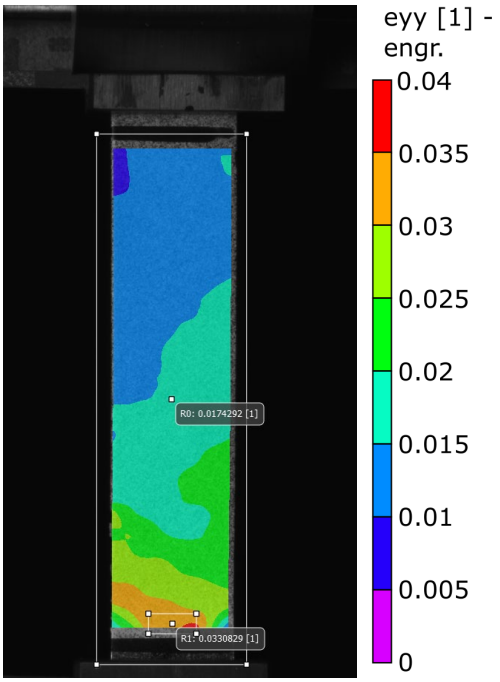

Fig. 16 Strain profile for typical Al foil paper-cut MD tensile specimen just before failure. The larger white box represents the gage length areal average, while the smaller white box represents the area where the strain concentration data is obtained.

Table 6 summarizes the tensile properties of Al foil from this study, as well as reference and literature values from other studies and sources. The referenced studies and sources did not claim use of optical methods to quantify specimen strain or perform a detailed examination of specimen fabrication technique and its effect on specimen edge quality.

Table 6 Summary of tensile material properties for Al foil from this study and literature

Source	Orientation (if given)	Modulus (GPa)	Yield stress (MPa)	Yield elongation (%)	Strength (MPa)	Elongation (%)
This study	MD	65.6	191.3	0.5	212.8	3.0
	TD	65.4	207.2	0.5	224.3	3.3
Klein et al. (2001) Al rolled and HT, 50 µm	…	69.1	…	…	…	4.2
Zhou et al. (2007) Al alloy 3003 rolled, 100 µm	…	…	…	…	190–195	…
MatWeb Al 1100-H19 foil (n.d.)	…	68.3	165.0	…	205.0	3.0

4.5 Brass Foil

The brass foil exhibited anisotropic behavior in tension with significant differences in the elastic and yield properties. Figure 17 shows the material response results for the four brass foil tensile experiments using paper-cut specimens in the (a) roll and (b) transverse orientations. The brass foil specimens failed at an elongation that was significantly lower than the reference values for this material, with correspondingly lower strength values; this is likely due to the presence of edge flaws.

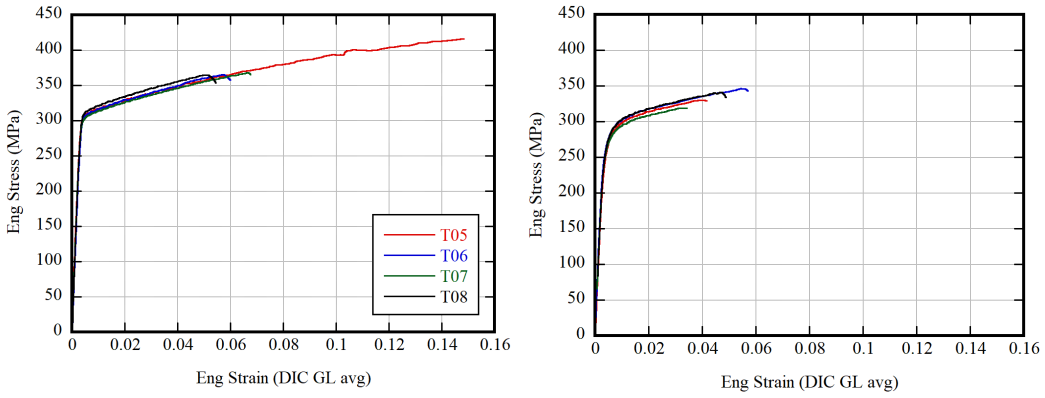

Fig. 17 Material response for tensile specimens of paper-cut brass foil in (a) MD and (b) TD orientations

The brass foil specimens exhibited strain uniformity in the gage length until failure, and the gage length average was used for strain measurement. At failure, the specimens exhibited stable crack growth, where a notch would begin to form and slowly grow across the specimen gage length for 5–10 s. Figure 18 shows the gage

length strain distribution at the time just prior to failure and notch formation for one typical brass foil MD tensile experiment.

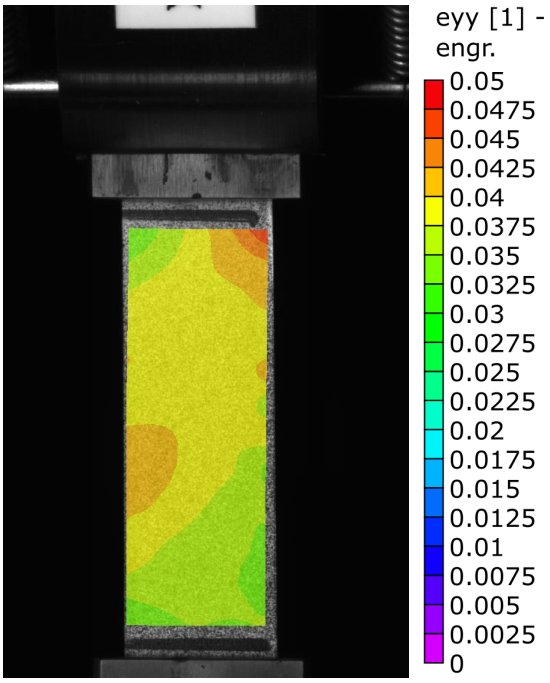

Fig. 18 Strain profile for typical brass foil paper-cut MD tensile specimen just before failure

Table 7 summarizes the tensile properties of brass foil from this study, as well as reference values obtained from other sources. No studies could be found on the tensile properties of this material. For brass, the references list single values and do not differentiate based on orientation.

Table 7 Summary of tensile material properties for brass foil from this study and literature

Source	Orientation (if given)	Modulus (GPa)	Yield stress (MPa)	Yield elongation (%)	Strength (MPa)	Elongation (%)
This study	MD TD	105.9 88.8	316.2 274.5	0.5 0.5	388.3 334.2	8.0 4.4
Material datasheet (United States Brass & Copper 2021)	…	…	235–320	…	430–450	26–37
MatWeb cartridge brass, 260 Brass, H02 temper	…	110.0	360.0	…	425.0	23.0

5. Conclusions

Experimental techniques to fabricate tensile specimens were developed for a range of high-performance polymer films and metallic foils. Experimental techniques to conduct tensile experiments on the films and foils were developed at quasi-static strain rate. Optical techniques were developed to quantify specimen strain and evaluate strain uniformity during loading. The material properties obtained in this study match or exceed the material properties published in references and literature studies. The failure behavior of films and foils is dependent on the specimen fabrication technique and, specifically, to the edge quality and presence and size of edge flaws. The tensile behavior of polyimide film, Al foil alloy 1100 temper H19, and PEI were found to be isotropic, with material properties for both MD and TD orientations very similar. PET film and brass foil alloy 260 were found to be anisotropic, with tensile properties significantly different for the roll and transverse directions.

The results demonstrate that tensile testing of films and foils is nontrivial and requires careful specimen preparation to generate tensile behavior that approaches the intrinsic material properties. For polymer films, the use of a bladed CNC cutter to produce dogbone specimens was found to result in the smoothest edges and highest elongation. In addition, the use of DIC strain measurement allows us to directly observe material strain without inaccuracies due to load frame compliance or specimen slip. The resulting polymer material properties, including modulus, strength, and elongation, are similar or higher than previously published values; prior studies likely suffered from specimen preparation and testing limitations that contained system compliance and premature specimen failure. For the metal foils, no method for dogbone preparation was found to produce suitable edge quality. Therefore, rectangular blade-cut specimens were used; results for these were similar or lower than reference values.

The quantified tensile material properties for polyimide, PEI, PET, Al foil, and brass foil will be useful for benchmarking mechanical characterization methods under development, including macroscale and microscale puncture, membrane pressurization, and high-rate puncture. These properties are currently being utilized in finite element simulations of complex loading of films and foils. These best practices for tensile testing will also prove valuable for evaluation of novel high-performance polymer and metallic films, and benchmarking performance relative to conventional films and foils.

6. References

Askins DR. Hydrolytic degradation of Kapton film. J Plastic Film Sheet. 1985 Jan;1(1):50–9.

ASTM D882-18. Standard test methods for tensile properties of thin plastic sheeting. Annual book of ASTM standards. ASTM International; 2018.

ASTM D6287-17. Standard practice for cutting film and sheeting test specimens. Annual book of ASTM standards. ASTM International; 2017.

ASTM E345-16. Standard test methods of tension testing of metallic foil. Annual book of ASTM standards. ASTM International; 2016.

Bhushan B, Ma T, Higashioji T. Tensile and dynamic mechanical properties of improved ultrathin polymeric films. J Appl Polym Sci. 2002 Mar 7;83(10):2225–44.

Chirkov SV, Kechekyan AS, Belov NA, Antonov SV, Alentiev AY. The influence of uniform deformation of Ultem-1000 polyetherimide films on their mechanical and gas transport characteristics. Petro Chem. 2016 Nov;56:1074–84.

Connolley T, Mchugh PE, Bruzzi M. A review of deformation and fatigue of metals at small size scales. Fatigue Fract Eng Mater Struct. 2005 Dec;28(12):1119–52.

CS Hyde Company. 36-F ULTEM 1000; n.d. [accessed 2023 Aug 29]. https://catalog.cshyde.com/Asset/Data%20Sheet%2036-F%20ULTEM%C2%AE%20Film.pdf.

DuPont. DuPont Kapton HN; n.d. [accessed 2023 Aug 28] https://www.dupont.com/content/dam/dupont/amer/us/en/ei-transformation/public/documents/en/EI-10206-Kapton-HN-Data-Sheet.pdf.

DuPont Teijin Films. Mylar polyester film; 2003 June [accessed 2023 Aug 29]. https://usa.dupontteijinfilms.com/wp-content/uploads/2017/01/Mylar_Physical_Properties.pdf.

Johnson RO, Burlhis HS. Polyetherimide: a new high-performance thermoplastic resin. Journal of Polymer Science: Polymer Symposia; 1983. vol. 70, no. 1, p. 129–143. Wiley.

Klein M, Hadrboletz A, Weiss B, Khatibi G. The ‘size effect’ on the stress–strain, fatigue and fracture properties of thin metallic foils. Mater Sci Eng A. 2001 Dec 1;319:924–8.

Kumar K, Pooleery A, Madhusoodanan K, Singh RN, Chatterjee A, Dutta BK, Sinha RK. Optimisation of thickness of miniature tensile specimens for evaluation of mechanical properties. Mater Sci Eng A. 2016 Oct 15;675:32–43.

Liu YA, Liu YA. Experimental research on uniaxial tensile mechanical properties of Kapton foils. J Polym Res. 2022 July;29(7):271.

MatWeb. Aluminum 1100-H19 foil; n.d. [accessed 2023 Aug 28]. http://www.matweb.com/search/DataSheet.aspx?MatGUID=2ca5a0592e4147848bdbd40d1ff1a056.

MatWeb. Cartridge brass, UNS C26000 (260 brass), H02 temper flat products; n.d. [accessed 2023 Aug 28]. https://www.matweb.com/search/DataSheet.aspx?MatGUID=89ddb61d3365402ea8bd8d4fe8462d43.

MatWeb. DuPont Kapton 200HN polyimide film, 50 micron thickness; n.d. [accessed 2023 Aug 28]. http://www.matweb.com/search/datasheet_print.aspx?matguid=46461ce29078477daf39c20f499e0bc8.

MatWeb. DuPont Teijin Films Mylar A polyester film, 200 gauge; n.d. [accessed 2023 Aug 29]. DuPont Teijin Films Mylar® A Polyester Film, 200 Gauge (matweb.com).

MatWeb. MatWeb Quantum PEI – Ultem; n.d. [accessed 2023 Aug 28]. https://www.matweb.com/search/DataSheet.aspx?MatGUID=3098d8dc04a64b6685fd24d28d8f677f.

Miyauchi M, Kazama KI, Sawaguchi T, Yokota R. Dynamic tensile properties of a novel Kapton-type asymmetric polyimide derived from 2-phenyl-4, 4′-diaminodiphenyl ether. Polym J. 2011 Oct;43(10):866–8.

Mouralova K, Bednar J, Benes L, Plichta T, Prokes T, Fries J. Production of precision slots in copper foil using micro EDM. Sci Rep. 2022;12(1):5023.

Roe JM, Baer E. Correlation of tensile properties of tough amorphous polymers with internal friction. Int J Polym Mater. 1972 Jan 1;1(2):133–46.

Schreier H, Orteu JJ, Sutton MA. Image correlation for shape, motion and deformation measurements: basic concepts, theory and applications. Springer-Verlag; 2009.

Shen Z, Mu Y, Ding Y, Liu Y, Zhao C. Study on the mechanical property of polyimide film in space radiation environments. Proc. SPIE 9796, Selected Papers of the Photoelectronic Technology Committee Conferences; 2016 Nov. p. 211–216.

Stearne JM, Ward IM. The tensile behaviour of polyethylene terephthalate. J Mater Sci. 1969 Dec;4:1088–96.

United States Brass & Copper. Alloy 260 1/2 hard temper product certification; 2021 Apr 16.

Zhang S, Mori S, Sakane M, Nagasawa T, Kobayashi K. Tensile properties and viscoelastic model of a polyimide film. J Solid Mech Mater Eng. 2012;6(6):668–77.

Zheng P, Chen R, Liu H, Chen J, Zhang Z, Liu X, Shen Y. On the standards and practices for miniaturized tensile test–a review. Fusion Eng Des. 2020 Dec 1;161:112006.

Zhou J, Shan DB, Guo B, Ma DL. Experimental study on specimen and grain size effects in uniaxial tension test of aluminum foil. Key Eng Mater. 2007 Aug 9;344:777–82.

List of Symbols, Abbreviations, and Acronyms

Al	aluminum
ASTM	American Society for Testing and Materials
CNC	computer numerical control
DIC	digital image correlation
EDM	electrical discharge machining
LED	light-emitting diode
MD	machine direction
PC	polycarbonate
PEI	polyetherimide
PET	polyethylene terephthalate
TD	transverse direction

1 (PDF)	DEFENSE TECHNICAL INFORMATION CTR DTIC OCA
1 (PDF)	DEVCOM ARL FCDD RLB CI TECH LIB
2 (PDF)	DEVCOM ARL FCDD RLA MD E WETZEL FCDD RLA TB CA GUNNARSSON